ASNT Research Symposium 2019, April 1st - 5th 2019, Hyatt Regency Orange County, Garden Grove, California

# High Resolution SCC Depth Map in Pipeline Samples Using New X-Ray Imaging Techniques

**Yohan Belanger[1,2], Luc Perron[2], and Xavier P. V. Maldague[1]**

[1]Université Laval
Département de génie électrique et de génie informatique
1065, av. de la Médecine, bureau 1300
Québec, Qc, Canada, G1V 0A6
(418) 656-2984; yohan.belanger.1@ulaval.ca

[2]LynX Inspection
2740 Rue Einstein
Québec, Qc, Canada, G1P 4S4
(418) 657-7706; ybelanger@lynxinspection.com

## ABSTRACT

Materials in pipelines are subjected to a series of stress and corrosive environments. These conditions eventually lead to stress corrosion cracking (SCC). Several NDT techniques already exist to detect and assess such cracks in the field, some being more efficient than others at providing accurate depth measurements. Depth measurements are essential to help decide between a low-cost repair and an expensive section replacement, but any new NDT method first needs to be evaluated in the lab before its gets deployed in the field. Validating that the method provides trustworthy results can hardly be done without a reliable ground truth. A new low cost X-Ray imaging method, involving scatter corrections and the physical aspects of SCC, was developed to generate high resolution 3D SCC depth maps of pipeline samples showing precise crack positions and depth measurements. This method could be used as a gold standard for evaluating traditional NDT techniques, such as ultrasound or eddy current, since digital X-Ray imagery in a controlled laboratory environment can yield better resolution. We will discuss the challenges of making such measurements and the techniques used to overcome them using state of the art hardware and software.

**Keywords:** Digital Radiography, DR, X-ray, Computer Vision, SCC, Pipelines

## INTRODUCTION

Pipeline transport is a method of long-distance transportation for fluids. They are often used to transport hydrocarbons and chemicals, but can also be used to transport water or any other liquid and gaseous products. Because pipelines are used for large volumes of fluids, any failure can have dramatic consequences. This is where non-destructive testing (NDT) can play a big role in finding preventable defaults. One such default is Stress Corrosion Cracking (SCC). It is defined as the growth of crack formation in a corrosive environment. Several NDT techniques can be used to spot such formations in the field. Newer techniques aim to find the depth of those formations in order to help decide between a low-cost repair and an expensive section replacement.

In this paper, we will talk about new radiography imaging techniques that can provide a high resolution map of cracks in a pipeline sample, both in position and in depth. These techniques use a combination of X-Ray Physics and Computer Vision in order to get the most information out of pipeline samples. In time, we want to verify that these non destructive techniques can be used to produce ground truth data to help assess in a laboratory environment other NDT solutions that are designed to be deployed in the field. We will detail the materials and methods, explain the theory behind them and discuss our results.

# THEORY

## Radiation Physics

Here are the primary effects that have an impact on image quality and thickness calibration.

### *X-Ray attenuation*

The major interactions causing X-Ray attenuation are the Photoelectric Effect, Compton Scattering and Pair Production. However, in the energy ranges that were used in this experiment, only the Photoelectric Effect and Compton Scattering should occur (Figure 1a). In reality, instead of computing the total cross-section of those two interactions, we use the Linear attenuation coefficient. This coefficient depends on the energy of the beam and the material it is going through(Figure 1b). Note here that the Linear attenuation coefficient is the Mass attenuation coefficient times the material's density.

**(Eq.1)** $I = I_0 e^{-\mu x}$

Where:

$I$ = Output beam intensity

$I_0$ = Input beam intensity

$\mu$ = Linear attenuation coefficient

$x$ = Distance travelled in the material

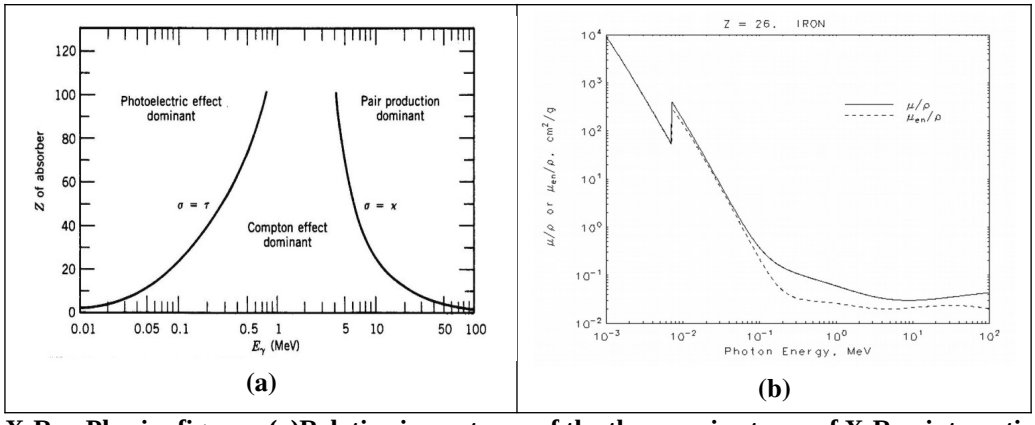


**Figure 1: X-Ray Physics figures. (a)Relative importance of the three major types of X-Ray interactions(1). (b)Example of X-Ray Mass attenuation coefficient(2).**

In practice, the end result depends on the integral of the attenuation coefficient over the spectrum of the source and the materials the beam is going through. It is however possible to see from Eq.1 that material thickness predictions based on beam intensity ratios are possible if these intensities are obtained in the exact same conditions as the calibration piece.

### *Compton Scattering*

At the energy range used in this experiment, Compton Scattering is the first interaction most photons will encounter when going through the sample. It is a lossy interaction that changes the path and the energy of the incident photon and produces a recoil electron that escapes with part of the incident energy. The energy of the outgoing photon is given by(1):

**(Eq. 2)** $$E_{\gamma'} = \frac{E_\gamma}{1 + (E_\gamma / m_e c^2)(1 - cos\theta)}$$

Where:

$E_{\gamma'}$= Outgoing photon energy

$E_\gamma$= Incident photon energy

$m_e$= Electron rest mass

$c$ = Speed of light

$\theta$= Scattering angle

As it is possible to see, the energy of the outgoing photon depends on the scattering angle. This means that in a given material, the scattered photons that have a narrow angle will keep most of their incident energy and be able to go through the sample with a wrong angle. This wrong angle is in turn one of the reasons, along with the focal spot size of the source, for visual blurring. This means that if you have a cradle that has a too much absorbent material, the contrast lines created in the sample will be blurred before entering the detector. It is possible to see the extent of this effect by looking at the angular differential cross-section of a single photon scattered from a single free electron, also named the Klein-Nishina formula(Figure 2).

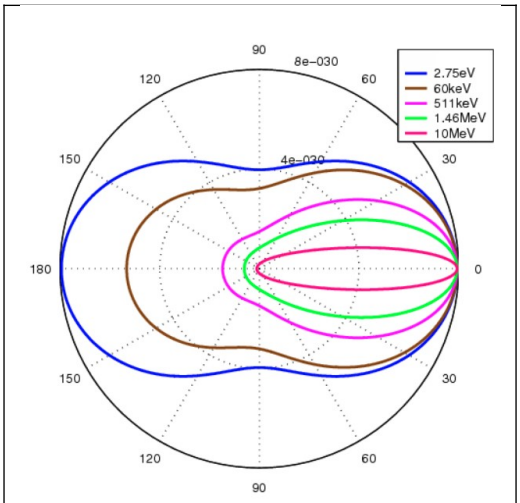


**(a)**

**Figure 2: Klein-Nishina distribution of scattering-angle cross sections over a range of commonly encountered energies.**

***Corrosion effects on X-Ray attenuation***

Most of the photons going through the sample will eventually be stopped by the Photoelectric Effect. Indeed, when looking at the proportionality of its cross section for photons with energies above the highest atomic binding energy, it is possible to see the relation between the Photoelectric Effect, the atomic number and the incident energy of the photon.

**(Eq. 3)** $$\sigma \propto \frac{Z^n}{E^m}$$

Where:

$\sigma$ = Approximate cross section

$Z^n$= Atomic number (with n≈4 at 0.1 MeV and n≈4.6 at 3 MeV)

$E^m$ = Energy of the incident photon (with m≈3 at 0.1 MeV and m≈1 at 5 MeV)

As it is possible to see from this equation, the photoelectric effect decreases steeply with the energy of the incident photon leaving room for compton scattering at higher energies. It also increases steeply with the atomic number of the material. (1).

Without going into the chemical details of corrosion, this process results in the bounding of lighter elements (like Oxygen or Chlorine) to the steel of the pipeline. From a radiation physics viewpoint, corrosion has the effect of lowering the effective atomic number of the samples, meaning that the photoelectric effect will be less effective at stopping radiation. It will have the effect of making parts of the samples appear thinner in the captured images.

## MATERIAL AND METHODS

In this section we will discuss the experimental setup and the methods used to clean the images.

### Experimental Setup

***X-Ray Source***

We used a 150 kV, 500 µA X-Ray source with a focal spot size of around 50 µm. It is a cone-beam source with a solid angle of 45° and using a constant potential (as opposed to to a pulsed beam). In this experiment, the applied potential ranged from approximately 100 kV to 150 kV and the current from approximately 300 µA to 500 µA.

***X-Ray Imaging Detector***

We used a detector equipped with an array of CMOS sensors coupled with a GadOx scintillator that produced 14 bpx images. The size of the array was 3096 x 3100 pixels with a resolution of 0.099 mm. The active area was 306 x 307 mm and could record images at 30 fps using two Camera Link cables. The source was placed at about 550 mm above the detector. We made sure that the detector array was circumscribed by the circle of the cone beam, meaning that the beam completely covered its active area.

***Linear translation stage***

We used a high precision, high accuracy 2D linear translation stage that moved on a set of rails mounted on an optics table. The height of the sample was set with a sturdy assembly of aluminum pegs bolted to the head of the moving cradle assembly.

***Radiography Cabinet***

We used a lead-lined NDT cabinet that was rated for the dose-rate of our source and met the radiation safety requirements of the Canadian Nuclear Safety Commission (CNSC).

***Pipeline samples***

The pipeline samples were provided by a local NDT company and had already been inspected using magnetic particle inspection, meaning the cracks were visible on the sample. Their size was around 200 x 100 mm and were made from very corroded X52 steel with varying thicknesses from ?? to ?? mm. A separate sample made of the same steel contained a series of thin EDM notches with distinct pre-defined depths was used as a reference. All samples were scanned at a height of approximately 320 mm above the detector array lying on an extruded polystyrene sheet.

***Software used***

Most of the software we used was based on open source libraries. Image processing and analysis was done using a combination of custom Python and C++ software utilities. Additional software tools were developed in Python and C++ to streamline the data analysis process. Some of the more detailed analysis required manual interventions.

## Methods

In this section we will discuss the methods we used for image production, processing/cleaning and analysis.

***Image acquisition***

We used the intrinsic geometrical magnification of our X-Ray setup to increase the resolution of the images and make the cracks more visible. As a result, the sample size exceeded considerably the available field of view of the detector which lead to the development of a custom image stitching algorithm. This algorithm automatically stitched all of the images together based on the given height of the sample and its relative XY position on the linear stage. To reduce the effects of noise and the geometric magnification of the penumbras in the images, we captured many images at every position and used the averaged result.

***Image pre-processing***

Detector background noise and intensity discrepancies caused by the source's heel effect were cleaned by using a custom polynomial gain and offset correction algorithm. We then removed the bad sensors by using a bilinear filter and rescaled the images to 16 bpx to facilitate processing. This process chain, which was repeated with every averaged image received from the detector, could be compared in essence to a flat field correction.

***Depth calibration***

We used a custom-made step wedge made out of a plate of X52 steel. The wedge was machined with steps ranging from 1 to 9 mm in height and 12 mm in length. The wedge was used as an intensity to thickness calibration piece. We were able to reduce the effects of X-Ray scattering by isolating each step of the wedge with other steel plates during capture. This effectively receded the edge effects and it was decided that the samples were to be scanned in this manner also. During this exercise we also found out that using polystyrene as the cradle base for the samples was prefered over a polyethylene base as it reduced diffusion blurring. We very carefully scanned each step and got the grey value to thickness curve from which we could start our work.

***Depth analysis***

We first started by verifying that the thickness curve we got from the step wedge was self consistent and could predict thickness well enough to verify the depth of the EDM notches on our machined sample. The thickness curve was applied to the stitched images of the pipeline samples and we started the analysis. We used a rolling-ball background subtraction algorithm that could attenuate the error caused by the curvature of the sample. We later applied a correction that took into account the degree of corrosion around the cracks. This correction is based on X-Ray attenuation physics and the change in effective atomic number of steel after being corroded.

## RESULTS

In this section we will discuss the results obtained from the calibration plate and the samples.

## Crack Depth

***EDM notched plate***

The first results came from the EDM machined plate with cavities of known depths. This plate was not corroded so we could test our image processing and depth finding algorithms on it. We had values for multiple notches but only a few will be presented here. The analysed depths were between 1 and 3 mm. The resulting images of each analysed EDM notches are presented in Figures 4 and 5. The structures on the left and the right of the highlighted cavities are other cavities with known depths, they appear faded because they were not centered in the image when it was captured and the curvature of the sample affected their contrast.

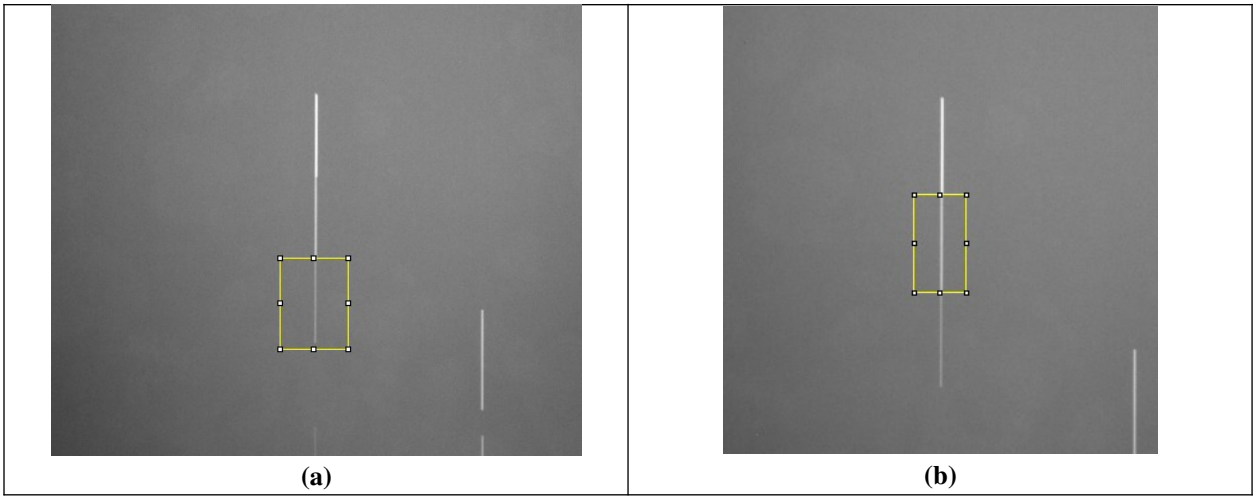

**(a)** **(b)**

**Figure 4: (a) Notch #2, 1 mm depth (b) Notch #3, 2mm Depth**

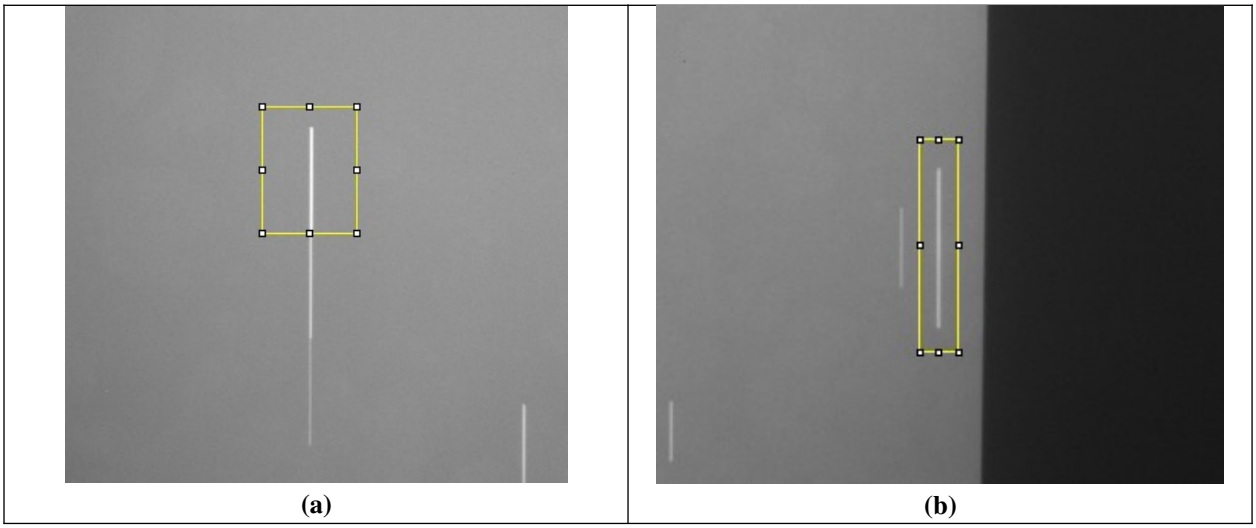

**(a)** **(b)**

**Figure 5: (a) Notch #4, 3 mm depth (b) Notch #11, 1mm Depth**

**Table 1: Predicted EDM notches depth and calibrated X-Ray measurements**

| Notch # | EDM depth | Measured Depth | Absolute Error | Relative Error |
|---|---|---|---|---|
| 2 | (1.00 ± 0.05) mm | 0.938 mm | 0.063 mm | 6.67 % |
| 3 | (2.00 ± 0.05) mm | 2.166 mm | 0.166 mm | 7.68 % |
| 4 | (3.00 ± 0.05) mm | 2.863 mm | 0.137 mm | 4.79 % |
| 11 | (1.00 ± 0.05) mm | 0.982 mm | 0.018 mm | 1.83 % |

Having these results in hand, we were ready to analyse an actual pipeline sample.

***Pipeline Sample***

Several samples were thoroughly analysed during this research, but for simplicity, we will focus in this paper on the results from only one of these samples. The experiments and analysis of this sample were repeated enough to ensure the repeatability of the methods. For a better understanding of the regions of interest in the sample (ROI), we will start by showing in Figure 6 the full stitched depth map of the sample with highlighted ROIs and then move on to the analysis of each individual region.

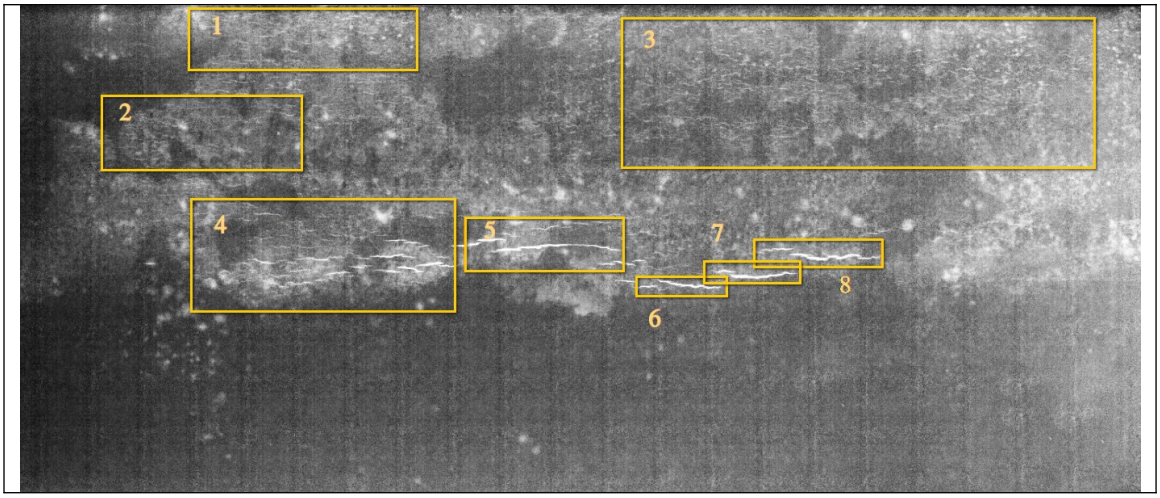


**Figure 6: Full depth map of the sample**

In Figure 7 we can see a high resolution version of region 2. It is possible to see first hand the effect of corrosion on the images, as a kind of white cloud that envelops the cracks.

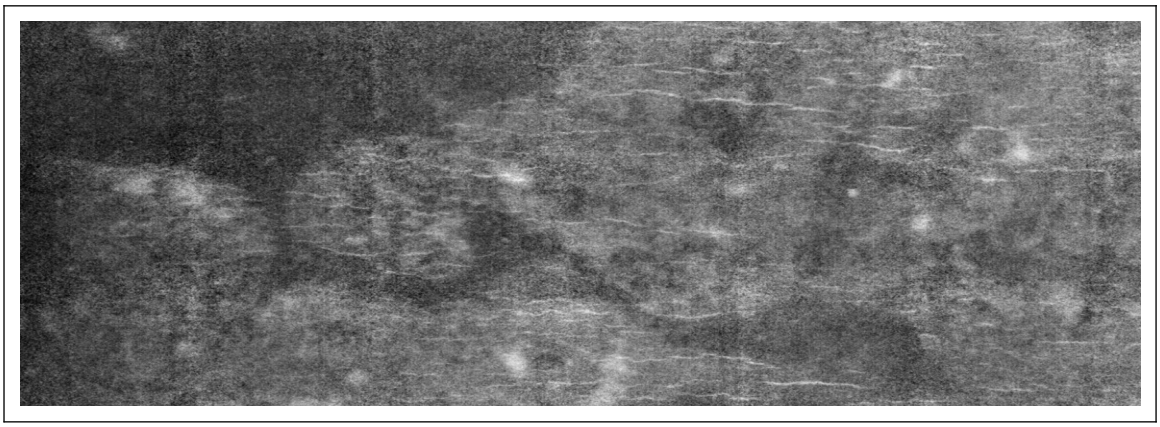

**Figure 7: Zoomed depth map of Region 2**

Table 2 compares the data we measured with data obtained from an Eddy Current analysis provided by the same NDT company that gave us the samples to see where our results stand against other techniques. Unfortunately we were not able to have the real depth measurement to test our data, as it would have to be taken with a destructive evaluation technique and the samples were not our own. In table 2 we will see the maximum depth data obtained from X-Ray for each of the defined regions in Figure 6.

**Table 2: SCC Depth for each of the defined regions**

| Region # | Maximum Depth | Maximum Depth with Corrosion Correction |
|---|---|---|
| 1 | (1.000 ± 0.090) mm | (1.764 ± 0.127) mm |
| 2 | (0.981 ± 0.091) mm | (1.771 ± 0.131) mm |
| 3 | (1.127 ± 0.140) mm | (1.959 ± 0.186) mm |
| 4 | (1.274 ± 0.125) mm | (2.102 ± 0.185) mm |
| 5 | (1.964 ± 0.145) mm | (2.813 ± 0.190) mm |
| 6 | (1.289 ± 0.086) mm | (2.092 ± 0.120) mm |
| 7 | (1.368 ± 0.104) mm | (2.195 ± 0.135) mm |
| 8 | (1.696 ± 0.100) mm | (2.525 ± 0.129) mm |

***3D Depth Map***

We were also able to produce a 3D depth map of the cracks. Since the corrosion correction is now mostly done by hand and is local to each crack, the results were rescaled for a better view and are only qualitative.

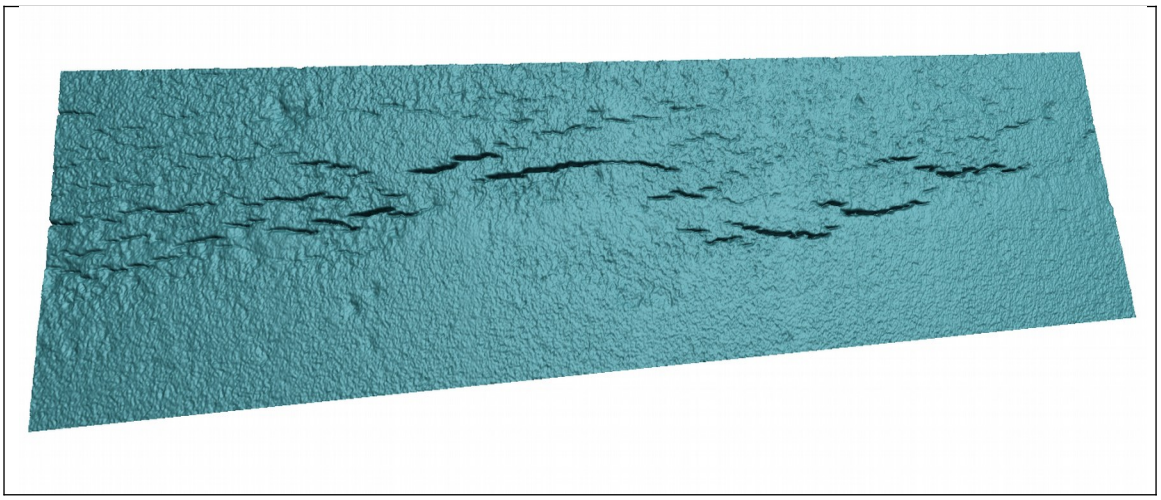

**Figure 10: Overhead view of the 3D depth map**

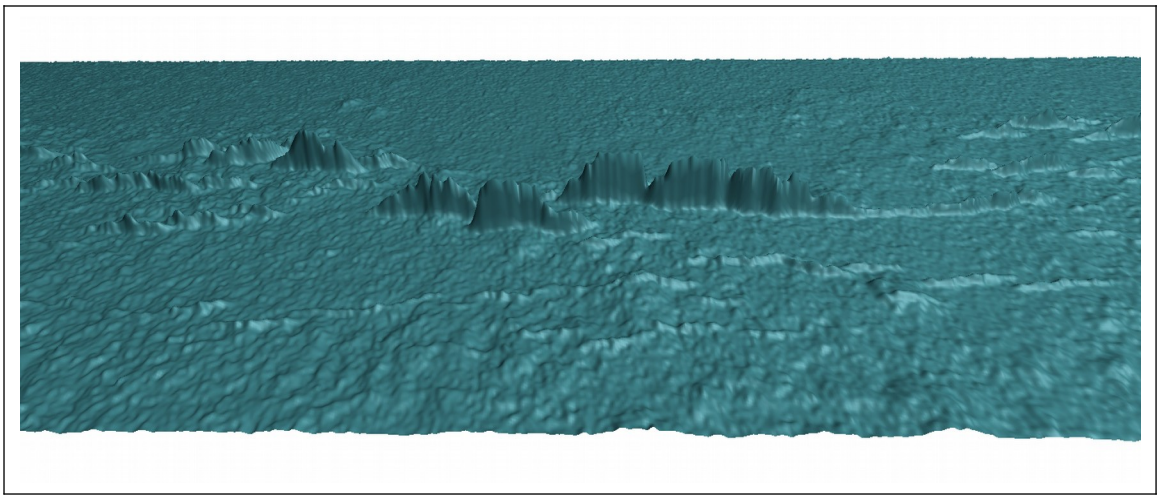

**Figure 11: Underneath view of the 3D depth map**

## DISCUSSION

### Precision and Accuracy of results

***Comparison to other methods***

To verify the validity of our results we compared them to results obtained from an Eddy Current analysis. Figure 12 shows a depth map from this analysis and Table 3 shows the values for the two methods side by side. It should be noted that the Eddy Current method cannot go deeper than 3 mm, that's why results deeper than that will be noted as 3+ mm.

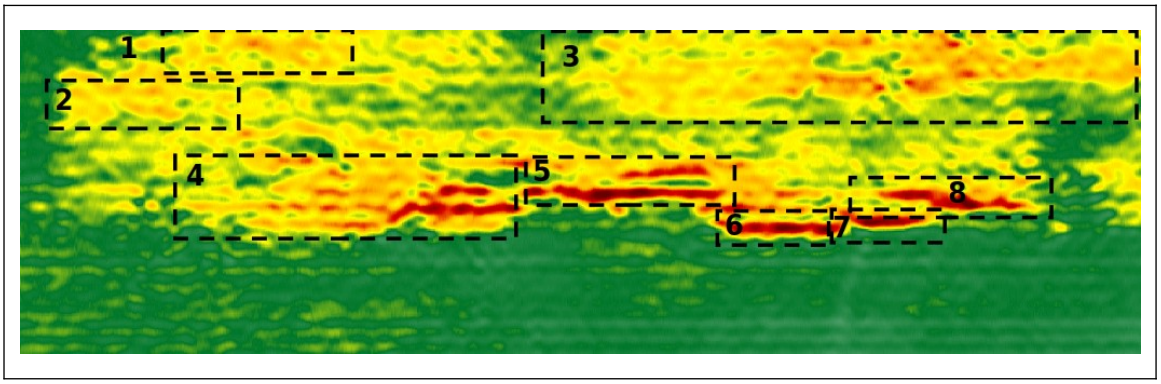


**Figure 12: Eddy Current analysis depth map**

**Table 3: Comparison between our data and Eddy Current analysis**

| Region # | This Article | Eddy Current | Difference |
|---|---|---|---|
| 1 | 1.764 mm | 1.0 mm | +0.764 mm |
| 2 | 1.771 mm | 0.9 mm | +0.871 mm |
| 3 | 1.959 mm | 1.3 mm | +0.659 mm |
| 4 | 2.102 mm | 2.4 mm | -0.298 mm |

| | | | |
|---|---|---|---|
| 5 | 2.813 mm | 3+ mm | -0.187 mm (+) |
| 6 | 2.092 mm | 2.2 mm | -0.108 mm |
| 7 | 2.195 mm | 2.5 mm | -0.305 mm |
| 8 | 2.525 mm | 3+ mm | -0.475 mm (+) |

## Error Analysis

In this part, we will review the factors that impacted our results and discuss their implications.

***Shape of samples***

An error factor that came up right at the start is the fact that the samples, coming from a pipeline, were having an ellipsoidally curved shape. While we used image stitching to reduce the effect of the cone beam divergence, we couldn't find a stable way to place the samples so that the beam crossed the exact same amount of material in each parts of the stitched image. This is especially true when trying to correct for corrosion on the up and down edges of the plate. It can be seen as the overshoot in the data comparisons for regions 1, 2 and 3. We usually come to find shallower cracks than Eddy Current analysis.

***Orientation of cracks***

Since X-Ray imaging is basically a measure of the path length of the beam in the sample, finding the perfect orientation of the sample for the beam to reach the bottom of the cracks was a challenge in itself. That's why we used the cone beam in combination with the linear stage to get a series of different viewing angles to find the optimal view that would provide the deepest measurement for any given region. However, any crack that propagate at an angle that exceeds the maximum angle of the cone beam (i.e. +/- 22.5 degrees) would yield greater depth measurement errors.

***Penumbra width and blurring***

By placing the samples near the source we had a great advantage in resolution because of the intrinsic geometrical magnification of the system. However, this has also the adverse effect of widening the penumbras of the contrast changes in the images and ultimately blurring the images. Nevertheless, the overall quality of the resulting x-ray images and the fact that we were able to distinguish very small thin cracks from the background with very sharp edges demonstrates that blurring did not have much of an effect in this case.

***Thickness calibration errors***

While our experimental setup and image cleaning techniques enabled us to acquire very repeatable data, it is clear that the conversion from gray value to intensity to thickness is prone to errors. Shot noise amplitude variations originating from a change in temperature of the combination scintillator-detector, ray-angle distribution within a sub-image used to create the stitched image and machining errors are all examples of what could go wrong with the thickness calibration. That's why we used the distribution of depths within a ROI and repeated measurement and analysis to get the statistics and compute the uncertainties shown above.

## CONCLUSIONS

In conclusion, we were able to come up with an intensity to thickness curve that was self-consistent and repeatable. Since it was based on a gray value distribution, it provided statistics for error assessment and helped us to see the effect of parameter changes. We were able to use the best parameters for this study and test our thickness curve on a known-depth sample to assess its accuracy and precision. We then analysed real pipeline samples and found out the corrosion was clouding our results. By using deterministic radiation physics equations we were able to find a way to correct the depth of the cracks that were clouded by corrosion.

Our measurements were coherent with the Eddy Current analysis but delivered much more spatial resolution and could resolve cracks that were very close together. We think that the methods shown in this article are precise and repeatable enough to pave the way towards a calibration standard for the measurement of SCC crack depths in pipelines that does not involve sample destruction. In the future, we would like to use computer vision to build an algorithm that does the corrosion correction automatically. We also want to automate the whole pipeline sample scanning procedure and analysis so that anyone could easily use this method. Once the procedure is automated we intend to proceed with thorough testing with different materials and levels of corrosion. Finally, we would like to use destructive testing on a few samples to confirm our results and potentially find details that might have been overlooked.

## ACKNOWLEDGEMENTS

For the equipment, the use of custom made software and the financial support we would like to thank:
LynX Inspection Inc.
www.lynxinspection.com

For the opportunity, the samples and the Eddy Current analysis we want to thank:
EddyFi Technologies
www.eddyfi.com

I want to thank all the coworkers at LynX that helped with this research: Martin Lacasse, Dominique Boutet, Roger Booto, Charles Brillon and Vincent Boulet.

## REFERENCES

(1) Attix F., 2008, *Introduction to Radiological Physics and Radiation Dosimetry*, Wiley-VCH, New York, NY.
(2) Hubbell J.H., Seltzer S.M., *X-Ray Mass Attenuation Coefficients*, NIST Standard Reference Database Number 126, National Institute of Standards and Technology, Gaithersburg, MD, 5632, https://dx.doi.org/10.18434/T4D01F, (retrieved 03-07-2019).